EPS0164

CLEO CONF 95-27
July 24, 1995

Measurement of the Form Factors for $\bar{B}^0 \to D^{*+}\ell^-\bar{\nu}$

J. Gronberg,[1] C.M. Korte,[1] R. Kutschke,[1] S. Menary,[1] R.J. Morrison,[1] S. Nakanishi,[1] H.N. Nelson,[1] T.K. Nelson,[1] C. Qiao,[1] J.D. Richman,[1] D. Roberts,[1] A. Ryd,[1] H. Tajima,[1] M.S. Witherell,[1] R. Balest,[2] K. Cho,[2] W.T. Ford,[2] M. Lohner,[2] H. Park,[2] P. Rankin,[2] J.G. Smith,[2] J.P. Alexander,[3] C. Bebek,[3] B.E. Berger,[3] K. Berkelman,[3] K. Bloom,[3] T.E. Browder,[3*] D.G. Cassel,[3] H.A. Cho,[3] D.M. Coffman,[3] D.S. Crowcroft,[3] M. Dickson,[3] P.S. Drell,[3] D.J. Dumas,[3] R. Ehrlich,[3] R. Elia,[3] P. Gaidarev,[3] M. Garcia-Sciveres,[3] B. Gittelman,[3] S.W. Gray,[3] D.L. Hartill,[3] B.K. Heltsley,[3] S. Henderson,[3] C.D. Jones,[3] S.L. Jones,[3] J. Kandaswamy,[3] N. Katayama,[3] P.C. Kim,[3] D.L. Kreinick,[3] T. Lee,[3] Y. Liu,[3] G.S. Ludwig,[3] J. Masui,[3] J. Mevissen,[3] N.B. Mistry,[3] C.R. Ng,[3] E. Nordberg,[3] J.R. Patterson,[3] D. Peterson,[3] D. Riley,[3] A. Soffer,[3] P. Avery,[4] A. Freyberger,[4] K. Lingel,[4] C. Prescott,[4] J. Rodriguez,[4] S. Yang,[4] J. Yelton,[4] G. Brandenburg,[5] D. Cinabro,[5] T. Liu,[5] M. Saulnier,[5] R. Wilson,[5] H. Yamamoto,[5] T. Bergfeld,[6] B.I. Eisenstein,[6] J. Ernst,[6] G.E. Gladding,[6] G.D. Gollin,[6] M. Palmer,[6] M. Selen,[6] J.J. Thaler,[6] K.W. Edwards,[7] K.W. McLean,[7] M. Ogg,[7] A. Bellerive,[8] D.I. Britton,[8] E.R.F. Hyatt,[8] R. Janicek,[8] D.B. MacFarlane,[8] P.M. Patel,[8] B. Spaan,[8] A.J. Sadoff,[9] R. Ammar,[10] P. Baringer,[10] A. Bean,[10] D. Besson,[10] D. Coppage,[10] N. Copty,[10] R. Davis,[10] N. Hancock,[10] S. Kotov,[10] I. Kravchenko,[10] N. Kwak,[10] Y. Kubota,[11] M. Lattery,[11] M. Momayezi,[11] J.K. Nelson,[11] S. Patton,[11] R. Poling,[11] V. Savinov,[11] S. Schrenk,[11] R. Wang,[11] M.S. Alam,[12] I.J. Kim,[12] Z. Ling,[12] A.H. Mahmood,[12] J.J. O'Neill,[12] H. Severini,[12] C.R. Sun,[12] F. Wappler,[12] G. Crawford,[13] J.E. Duboscq,[13] R. Fulton,[13] D. Fujino,[13] K.K. Gan,[13] K. Honscheid,[13] H. Kagan,[13] R. Kass,[13] J. Lee,[13] M. Sung,[13] C. White,[13] A. Wolf,[13] M.M. Zoeller,[13] X. Fu,[14] B. Nemati,[14] W.R. Ross,[14] P. Skubic,[14] M. Wood,[14] M. Bishai,[15] J. Fast,[15] E. Gerndt,[15] J.W. Hinson,[15] T. Miao,[15] D.H. Miller,[15] M. Modesitt,[15] E.I. Shibata,[15] I.P.J. Shipsey,[15] P.N. Wang,[15] L. Gibbons,[16] S.D. Johnson,[16] Y. Kwon,[16] S. Roberts,[16] E.H. Thorndike,[16] T.E. Coan,[17] J. Dominick,[17] V. Fadeyev,[17] I. Korolkov,[17] M. Lambrecht,[17] S. Sanghera,[17] V. Shelkov,[17] T. Skwarnicki,[17] R. Stroynowski,[17] I. Volobouev,[17] G. Wei,[17] M. Artuso,[18] M. Gao,[18] M. Goldberg,[18] D. He,[18] N. Horwitz,[18] S. Kopp,[18] G.C. Moneti,[18] R. Mountain,[18] F. Muheim,[18] Y. Mukhin,[18] S. Playfer,[18] S. Stone,[18] X. Xing,[18] J. Bartelt,[19] S.E. Csorna,[19] V. Jain,[19] S. Marka,[19] D. Gibaut,[20] K. Kinoshita,[20] P. Pomianowski,[20] B. Barish,[21] M. Chadha,[21] S. Chan,[21] D.F. Cowen,[21] G. Eigen,[21] J.S. Miller,[21] C. O'Grady,[21] J. Urheim,[21] A.J. Weinstein,[21] F. Würthwein,[21] D.M. Asner,[22] M. Athanas,[22] D.W. Bliss,[22] W.S. Brower,[22] G. Masek,[22] and H.P. Paar[22]

(CLEO Collaboration)

[1] *University of California, Santa Barbara, California 93106*
[2] *University of Colorado, Boulder, Colorado 80309-0390*
[3] *Cornell University, Ithaca, New York 14853*
[4] *University of Florida, Gainesville, Florida 32611*
[5] *Harvard University, Cambridge, Massachusetts 02138*
[6] *University of Illinois, Champaign-Urbana, Illinois, 61801*
[7] *Carleton University, Ottawa, Ontario K1S 5B6 and the Institute of Particle Physics, Canada*
[8] *McGill University, Montréal, Québec H3A 2T8 and the Institute of Particle Physics, Canada*
[9] *Ithaca College, Ithaca, New York 14850*
[10] *University of Kansas, Lawrence, Kansas 66045*
[11] *University of Minnesota, Minneapolis, Minnesota 55455*
[12] *State University of New York at Albany, Albany, New York 12222*
[13] *Ohio State University, Columbus, Ohio, 43210*
[14] *University of Oklahoma, Norman, Oklahoma 73019*
[15] *Purdue University, West Lafayette, Indiana 47907*
[16] *University of Rochester, Rochester, New York 14627*
[17] *Southern Methodist University, Dallas, Texas 75275*
[18] *Syracuse University, Syracuse, New York 13244*
[19] *Vanderbilt University, Nashville, Tennessee 37235*
[20] *Virginia Polytechnic Institute and State University, Blacksburg, Virginia, 24061*
[21] *California Institute of Technology, Pasadena, California 91125*
[22] *University of California, San Diego, La Jolla, California 92093*

Abstract

Using a sample of 2.6×10^6 $\Upsilon(4S) \to B\bar{B}$ events collected with the CLEO II detector at the Cornell Electron Storage Ring, we have measured the form factors for $\bar{B}^0 \to D^{*+}\ell^-\overline{\nu}$. We perform a three-parameter fit to the joint distribution of four kinematic variables to obtain the preliminary form factor ratios $R_1 = 1.18 \pm 0.30 \pm 0.12$ and $R_2 = 0.71 \pm 0.22 \pm 0.07$, and the form-factor slope $\rho^2_{A_1} = 0.91 \pm 0.15 \pm 0.06$, which is closely related to the slope of the Isgur-Wise function. By using the large CLEO data sample and the correlations among the observed kinematic variables, we have measured for the first time all three parameters simultaneously. The form factor ratios are consistent with predicted corrections from the heavy-quark symmetry limit $R_1 = R_2 = 1$. In addition, we observe large effects due to interference terms in the decay rate that are consistent with a $V-A$ coupling at both W vertices.

---

[*] Permanent address: University of Hawaii at Manoa

I. INTRODUCTION

Semileptonic decays of hadrons containing a bottom quark provide a means both to measure fundamental parameters of the standard model—the magnitudes of the Cabibbo-Kobayashi-Maskawa mixing angles V_{cb} and V_{ub}—and to understand the effects of strong interactions on the underlying weak decays. These two problems are related, because accurate determination of CKM elements requires a good understanding of the decay dynamics [1]. The decay $B \to D^*\ell\nu$ is a key process for these studies. From a theoretical standpoint, it has been analyzed in detail [2–12], in the framework of heavy quark effective theory (HQET), in which the decay amplitude is expanded in powers of $1/m_b$ and $1/m_c$. Because the charm and bottom masses are reasonably large compared with the energies associated with strong interactions in the decay, both the masses and the spins of the heavy quarks are expected to play little role in the dynamics. These considerations lead to symmetry relations that significantly simplify the description of the process. For $B \to D^*\ell\nu$, HQET yields numerous predictions, some of which we are able to test using the detailed studies of decay distributions presented in this paper.

In calculations of exclusive semileptonic decays, the amplitude is expressed in terms of the available four vectors (momentum and spin-polarization vectors) and one or more form factors, which are Lorentz-invariant functions that depend only on q^2, the square of the mass of the virtual W. The form factors parametrize the effect of strong interactions on the decay. Calculations of charm and bottom semileptonic decay form factors have been based on the quark model [13–18] and, more recently, on lattice QCD methods [19,20] and QCD sum rules [21–25,8]. For light charged leptons ($\ell = e$ or $\ell = \mu$), the decay $B \to D^*\ell\nu$ depends on three form factors. Although HQET does not predict their q^2 dependence, it does relate these three form factors, up to relatively small corrections, to a single, universal form factor, called the Isgur-Wise function. The goal of this analysis is to both measure the q^2 dependence of the form factors and to test, in so far as possible, the predictions of these theoretical methods and models.

We study the form factors for $\bar{B}^0 \to D^{*+}\ell^-\overline{\nu}$ (charge-conjugate modes are implied throughout this paper) using the channel $D^{*+} \to D^0\pi^+$ with $D^0 \to K^-\pi^+$ or $D^0 \to K^-\pi^+\pi^0$. The integrated luminosity of the data sample is 2.404 fb^{-1} on the $\Upsilon(4S)$, which corresponds to $(2.579 \pm 0.018) \times 10^6$ $B\overline{B}$ pairs. We also use a 1.139 fb^{-1} data sample obtained at a center-of-mass energy about 60 MeV below the $\Upsilon(4S)$ to measure the continuum background. The data were collected using the CLEO II detector, which is described in detail elsewhere [26]. For this analysis, the most important features are the tracking system, which we use to measure charged-pion momenta down to about 60 MeV/c; the CsI calorimeter, which provides excellent photon and electron identification; and the muon system.

II. DECAY DISTRIBUTIONS AND FORM FACTORS FOR $\bar{B}^0 \to D^{*+}\ell^-\overline{\nu}$

The differential decay rate for $\bar{B}^0 \to D^{*+}\ell^-\overline{\nu}$, $D^{*+} \to D^0\pi^+$ can be expressed in terms of three q^2-dependent helicity amplitudes $H_\pm(q^2)$ and $H_0(q^2)$, where the subscripts refer to the helicity of either the virtual W or the D^{*+}. The rate is given by

$$
\begin{aligned}
\frac{d\Gamma(\bar{B}^0 \to D^{*+}\ell^-\overline{\nu},\ D^{*+} \to D^0\pi^+)}{dq^2\, d\cos\theta_\ell\, d\cos\theta_V\, d\chi} = {} & \frac{3G_F^2|V_{cb}|^2\, P_{D^*}\, q^2}{8(4\pi)^4 m_B{}^2}\mathcal{B}(D^{*+} \to D^0\pi^+) \times \\
& \{[(1-\cos\theta_\ell)^2|H_+(q^2)|^2 + (1+\cos\theta_\ell)^2|H_-(q^2)|^2]\sin^2\theta_V \\
& +4\sin^2\theta_\ell\cos^2\theta_V|H_0(q^2)|^2 \\
& -2\sin^2\theta_\ell\sin^2\theta_V\cos(2\chi)H_+(q^2)H_-(q^2) \\
& -4\sin\theta_\ell(1-\cos\theta_\ell)\sin\theta_V\cos\theta_V\cos\chi\, H_+(q^2)H_0(q^2) \\
& +4\sin\theta_\ell(1+\cos\theta_\ell)\sin\theta_V\cos\theta_V\cos\chi\, H_-(q^2)H_0(q^2)\},
\end{aligned} \tag{1}
$$

where m_B is the mass of B meson; P_{D^*} is the momentum of the D^* and is a function of q^2; $\mathcal{B}(D^{*+} \to D^0\pi^+)$ is the branching fraction for $D^{*+} \to D^0\pi^+$; and the angles θ_ℓ, θ_V, and χ are defined in Fig. 1. Note that θ_ℓ is defined with respect to the direction of the virtual W; this accounts for the sign differences between our formula and certain others in the literature [27]. Although some of these distributions have been studied previously [28–32], our analysis is the first to use all the information from all four kinematic variables (q^2, $\cos\theta_\ell$, $\cos\theta_V$, and χ) as well as the first to use their correlations, which are very powerful.

The helicity amplitudes $H_\pm$ and H_0 can be expressed in terms of two axial-vector form factors, $A_1(q^2)$ and $A_2(q^2)$, and a vector form factor $V(q^2)$:

$$
\begin{aligned}
H_\pm(q^2) &= (m_B + m_{D^*})A_1(q^2) \mp \frac{2m_B\, P_{D^*}}{(m_B+m_{D^*})}V(q^2) \\
H_0(q^2) &= \frac{1}{2m_{D^*}\sqrt{q^2}}\Big[(m_B^2 - m_{D^*}^2 - q^2)(m_B+m_{D^*})A_1(q^2) - \frac{4m_B^2\, P_{D^*}^2}{(m_B+m_{D^*})}A_2(q^2)\Big],
\end{aligned} \tag{2}
$$

where m_{D^*} is the mass of the D^* meson. As a result of the $V-A$ coupling, the probability for producing a negative helicity D^* is larger than that for producing a positive helicity D^*, and the difference $H_-(q^2) - H_+(q^2)$ is large over much of the q^2 range.

In studies of charm semileptonic decay, the shapes of the form factors are usually assumed to be governed by pole forms with pole masses taken from theory. In studies of $D \to K^*\ell^+\nu$, for example, these assumptions leave two remaining parameters, quoted at $q^2 = 0$, that govern the shapes of the distributions, $r_V = V(0)/A_1(0)$ and $r_2 = A_2(0)/A_1(0)$. Our study differs in two respects: we have enough data to determine three parameters and second, we choose our form-factor ratios somewhat differently.

In the heavy-quark symmetry limit, the form factors are related to the Isgur-Wise function ξ:

$$
V(q^2) = A_2(q^2) = \frac{A_1(q^2)}{\left[1 - \frac{q^2}{(m_B+m_{D^*})^2}\right]} = \frac{(m_B+m_{D^*})}{2\sqrt{m_B m_{D^*}}}\xi(w), \tag{3}
$$

where $w = (m_B^2 + m_{D^*}^2 - q^2)/(2m_B m_{D^*})$. The variable w is simply the relativistic factor γ for the D^* in the B-meson rest frame, ranging from 1 to about 1.5. Following Neubert [8], we define the form factor ratios

$$
R_1 \equiv \left[1 - \frac{q^2}{(m_B+m_{D^*})^2}\right]\frac{V(q^2)}{A_1(q^2)}
$$

$$R_2 \equiv \left[1 - \frac{q^2}{(m_B + m_{D^*})^2}\right] \frac{A_2(q^2)}{A_1(q^2)}. \tag{4}$$

These ratios (and not r_V and r_2) are predicted to be unity, independent of w, in the heavy-quark symmetry limit. For this reason, our fits use R_1 and R_2 rather than r_V and r_2. Furthermore, we fit for these values at the zero-recoil configuration $w = 1$ ($q^2_{\rm max}$) rather than $q^2 = 0$, since the hadronic system is least disturbed and theoretical predictions are most reliable in this region of phase space.

To allow departures from the heavy-quark symmetry limit but still express the form factors in a manner that makes this limit transparent, one can use

$$\begin{aligned}
A_1(q^2) &= \frac{m_B + m_{D^*}}{2m_B m_{D^*}}\left[1 - \frac{q^2}{(m_B + m_{D^*})^2}\right] h_{A_1}(w), \\
A_2(q^2) &= \frac{m_B + m_{D^*}}{2m_B m_{D^*}} R_2(w) h_{A_1}(w), \\
V(q^2) &= \frac{m_B + m_{D^*}}{2m_B m_{D^*}} R_1(w) h_{A_1}(w),
\end{aligned} \tag{5}$$

where $h_{A_1}(w) \to \xi(w)$ in the heavy-quark symmetry limit. Departures from this limit produce two effects: deviations of $R_1(1)$ and $R_2(1)$ from unity and a slight variation of R_1 and R_2 with w.

Ideally, the most general fit of the kinematic distributions would determine the arbitrary functions $R_1(w)$, $R_2(w)$, and $h_{A_1}(w)$ (or equivalently, $A_1(q^2)$, $A_2(q^2)$ and $V(q^2)$). However, until the data samples become much larger, it will be necessary to impose some constraints on the fit, as we discuss later in this paper.

It is common to report the values of certain other integrated observables that can be derived from the form factors. These are $\bar{A}_{\rm FB}$, the forward-backward asymmetry of the lepton in the W rest frame, and $\bar{A}_{\rm pol}$, which is related to the ratio of longitudinal to transverse polarization of the D^{*+}. They are given by $\bar{A}_{\rm pol} = 2(\Gamma_L/\Gamma_T) - 1$ and $\bar{A}_{\rm FB} = 3/4(\Gamma_- - \Gamma_+)/(\Gamma_L + \Gamma_T)$, where $\Gamma_L = \Gamma_0$, $\Gamma_T = \Gamma_+ + \Gamma_-$, and $\Gamma_i = (G_F^2|V_{cb}|^2/96\pi^3) \int dq^2 P_{D^*}(q^2/m_B{}^2)|H_i(q^2)|^2$.

III. EVENT SELECTION AND BACKGROUNDS

The event selection is designed to obtain a signal with low background, so that the systematic errors resulting from the modeling of backgrounds are minimized. The main backgrounds, starting with the largest, are from (1) combinatorial background (fake D^{*+}'s); (2) $B \to D^{**}\ell\nu$ or $B \to D^*\pi\ell\nu$ decays producing a real D^{*+} and D^0; (3) events in which the D^{*+} and the lepton are not from the same B meson (we call such events uncorrelated D^{*+}-ℓ pairs because the B mesons are produced nearly at rest, leading to uncorrelated momentum vectors for the D^{*+} and the lepton); (4) events in which a hadron has faked a lepton signature; and (5) continuum (non-$\Upsilon(4S)$ events).

We start with events satisfying the standard CLEO hadronic event criteria [34]. Each event is then required to contain at least one electron candidate with momentum P_ℓ in the range 1.0 GeV/c to 2.45 GeV/c, or at least one muon candidate with momentum in the range 1.4 GeV/c to 2.45 GeV/c. The lepton direction must be in the range $|\cos\theta| < 0.71$, where θ is the polar angle from the beam axis. Muon candidates are identified by the presence of muon chamber hits after at least 5 nuclear interactions lengths of material. This criterion produces an effective minimum cut on the muon momentum at about 1.2 GeV/c; we raise the cut to 1.4 GeV/c, where the efficiency is higher.

Continuum background is suppressed using an event-shape variable, R_2, equal to the ratio of the second to the zeroth Fox-Wolfram moments [35]. We require $R_2 < 0.3$, which selects more spherical rather than jet-like events.

We next search for D^0 signals in the modes $D^0 \to K^-\pi^+$ and $D^0 \to K^-\pi^+\pi^0$. In the first mode, no particle identification is required for the charged kaon and pion; besides loose track quality cuts, we require only that the candidates have opposite charges and that the kaon have the same charge as the lepton. For the three-body D decay, there is more combinatorial background, so we use dE/dx information from the drift chamber to help identify the kaon. The π^0 is identified using the CsI calorimeter: the photons are required to have energies of at least 50 MeV, the π^0 mass must be within 2σ of the nominal value, and the π^0 energy in the lab frame must exceed 350 MeV. The $D^0 \to K^-\pi^+$ candidates must have a $K^-\pi^+$ mass within 16 MeV/c^2 of the nominal D^0 value; $D^0 \to K^-\pi^+\pi^0$ candidates must have a $K^-\pi^+\pi^0$ mass within 25 MeV/c^2 of the nominal value. The D^0 candidates must have a lab-frame momentum P_{D^0} less than 2.45 GeV/c, which is close to the kinematic limit for D^*'s from B decays.

To further reduce the combinatorial background in reconstructing the three-body D decay, we use measurements of the $D^0 \to K^-\pi^+\pi^0$ Dalitz plot from E691 [36] to compute a probability weight for each $K^-\pi^+\pi^0$ combination. We require that this weight exceed a minimum value that selects the most likely 62% of $K^-\pi^+\pi^0$ population within the $D^0 \to K^-\pi^+\pi^0$ Dalitz plot. In events with more than one D^0 candidate, a best candidate is selected on the basis of the π^0 mass and the Dalitz amplitude.

We reconstruct charged D^* candidates by combining D^0's with additional charged tracks of momentum P_{π_s} at least 65 MeV/c. The charge of this pion candidate must be opposite to that of the lepton. We select D^* candidates in both channels by requiring that δm be within 2 MeV/c^2 of the nominal value.

To suppress events in which the D^{*+} and the lepton are produced in the decay chains of different B's (uncorrelated background), we require the D^{*+} and the lepton to be in opposite hemispheres. (This background produces D^*-lepton pairs with unlike charges if the lepton is primary and $B^0\bar{B}^0$ mixing has occurred, or if the lepton is secondary and no mixing has occurred.) If the D^{*+} and the lepton are produced in a $B \to D^*\ell\nu$ decay, they tend to be in opposite hemispheres, whereas the uncorrelated background is uniformly distributed in $\cos\theta_{D^*\ell}$, where $\theta_{D^*\ell}$ is the angle between the D^{*+} and the lepton in the lab frame.

The final step in the event selection is designed to exploit the fact that, in the decay $\bar{B}^0 \to D^{*+}\ell^-\overline{\nu}$, the kinematics of the decay must be consistent with the presence of a neutrino recoiling against the $D^{*+}\ell^-$ system. For a signal event, we expect $p^2_{\rm miss} = p^2_\nu = 0$, where

$$\begin{aligned} p^2_{\rm miss} &= (p_B - p_{D^*\ell})^2 \\ &= m^2_B + m^2_{D^*\ell} - 2E_B E_{D^*\ell} + 2|\mathbf{p}_B||\mathbf{p}_{D^*\ell}|\cos\theta_{B,D^*\ell} \end{aligned} \tag{6}$$

and $p_{D^*\ell} = p_{D^*} + p_\ell$. Although the angle $\theta_{B,D^*\ell}$ between the B and $(D^* + \ell^-)$ momentum directions is unknown, one can neglect the last term since $|\mathbf{p}_B| \approx 330$ MeV/c is small. Thus, we define

$$M^2_{\rm miss} = m^2_B + m^2_{D^*\ell} - 2E_B E_{D^*\ell}. \tag{7}$$

The quantity $M^2_{\rm miss}$ is appealing intuitively because background from $B \to D^{**}\ell\nu$, which produces an additional pion, peaks at larger values of $M^2_{\rm miss}$ than the signal. To suppress background from $B \to D^{**}\ell\nu$ we require $M^2_{\rm miss} < 0$ for events with electrons and $M^2_{\rm miss} < 0.7\ {\rm GeV}^2/c^4$ for events with muons. The muon channel has a looser cut because the higher momentum requirement in the muon channel already removes a substantial amount of the $B \to D^{**}\ell\nu$ background. The cuts are designed to reduce this background to about the same size in the electron and muon samples.

We can also impose the condition $p^2_{\rm miss} = 0$, which is satisfied for signal events, and solve Eq. 6 for $\cos\theta_{B,D^*\ell}$. The quantity $\cos\theta_{B,D^*\ell}$ computed in this way is highly correlated with the estimated value of $M^2_{\rm miss}$, but it allows us to precisely impose the kinematic consistency condition through the requirement $|\cos\theta_{B,D^*\ell}| \le 1$, which is satified by signal events up to small resolution effects. (The cut $M^2_{\rm miss} < 0$, used for electrons, corresponds to $\cos\theta_{B,D^*\ell} > 0$.) Figure 2 shows the δm distributions for the $D^0 \to K^-\pi^+$ and $D^0 \to K^-\pi^+\pi^0$ channels after all analysis cuts are applied except the δm cut.

	$K\pi\ e$	$K\pi\ \mu$	$K\pi\pi^0\ e$	$K\pi\pi^0\ \mu$	Total
Raw yield	267 ± 16	292 ± 17	192 ± 14	189 ± 14	940 ± 31
Fake D^*	17 ± 3	21 ± 4	20 ± 4	21 ± 4	79 ± 8
$B \to D^{**}\ell\nu$	12 ± 7	17 ± 8	8 ± 5	11 ± 5	48 ± 25
Uncorrelated	7 ± 4	3 ± 3	6 ± 3	0 ± 2	16 ± 6
Fake leptons	1 ± 1	6 ± 3	1 ± 1	5 ± 3	13 ± 6
Continuum	2 ± 2	3 ± 3	0 ± 2	0 ± 2	5 ± 5
Signal	228 ± 18	242 ± 20	157 ± 16	152 ± 16	779 ± 42

TABLE I. The yields in the $K\pi$ and $K\pi\pi^0$ channels and the estimated background contributions.

Table I lists the estimated number of events from each background and the signal. The largest background, which is from fake D^*'s, is only 10% of the signal. The number of such fake D^*'s is determined using the sideband region $0.15 < \delta m < 0.17$ GeV/c^2. The background from $B \to D^{**}\ell\nu$, though even smaller, has a larger uncertainty, since it consists of several contributing modes that are not completely understood. Our model for these background sources is based on a combination of results from the ISGW2 model and measurements from the ALEPH experiment [33]. In the ISGW2 model [14], the dominant resonant modes contributing to $B \to D^{**}\ell\nu$ are $B \to D_1\ell^-\overline{\nu}$ and $B \to D_2^*\ell^-\overline{\nu}$, whose branching fractions are expected to be in the ratio 2:1. The D_1 and D_2^* are orbitally excited ($L = 1$) charm mesons in which the light quark and the gluons have combined spin and orbital angular momentum $j = 3/2$. The model also predicts smaller rates for decays to two other orbitally excited charm mesons, those with $j = 1/2$, only one of which decays into $D^*\pi$. Our approach is to normalize the ISGW2 model using the ALEPH [33] measurement $\mathcal{B}(b \to B)\mathcal{B}(B \to D_1^0\ell^-\overline{\nu}X)\mathcal{B}(D_1^0 \to D^{*+}\pi^-) = (2.04 \pm 0.58 \pm 0.34) \times 10^{-3}$. We assume that this rate is dominated by the resonant component $B \to D_1^0 \ell^- \overline{\nu}$ to normalize the ISGW2 model. Furthermore, we add in nonresonant $B \to D^{*+}\pi^-\ell^-\overline{\nu}$ events so that the sum of all the resonant and nonresonant modes is equal to $(0.92 \pm 0.31)\%$, which we have derived from the ALEPH measurement $\mathcal{B}(b \to B)\mathcal{B}(B \to D^{*+}\pi^-\ell^-\overline{\nu}X) = (3.7 \pm 1.0 \pm 0.7) \times 10^{-3}$. Although the form factors for these modes have not been measured, we have a reasonably good idea of what their kinematic distributions are like, for reasons explained later in our discussion of the fits. Uncorrelated D^*-ℓ combinations, events with fake leptons, and continuum backgrounds are small, and the number of events in each case is determined from data. We discuss issues related to modeling the four-dimensional kinematic distributions for these backgrounds in the section on the fits.

IV. KINEMATIC VARIABLES AND ACCEPTANCE EFFECTS

To extract the form factors, we perform a fit to the joint distribution in the kinematic variables $\cos\theta_\ell$, $\cos\theta_V$, χ, and q^2. It is important to reconstruct these variables with the best possible resolution. The dominant source of smearing is the unknown direction of the B meson, which has a small velocity $\beta \approx 0.06$ in the lab frame. The effect of the B motion is especially important at high q^2, where the D^* moves slowly in the B rest frame; the boost from the B motion can then account for a substantial fraction of the observed D^* momentum.

Although there is not enough information to completely determine the direction of the B momentum vector, the direction of the B meson is constrained to lie on a cone of known opening angle with respect to $\mathbf{p}_{D^*\ell}$. The azimuth of $\mathbf{p}_B$ on this cone, however, cannot be determined. Within this constraint, we consider two extreme configurations, those with the largest and smallest opening angles between $\mathbf{p}_B$ and $\mathbf{p}_{D^*}$. These configurations correspond, respectively, to the smallest and largest values of q^2 consistent with the observed four-vectors, since

$$q^2 = (p_B - p_{D^*})^2 = m_B^2 + m_{D^*}^2 - 2(E_B E_{D^*} - |\mathbf{p}_B||\mathbf{p}_{D^*}|\cos\theta_{B,D^*}). \qquad (8)$$

Our method is to compute the values of q^2, $\cos\theta_\ell$, $\cos\theta_V$, and χ for each of these extreme configurations and to use the average as the estimate for each kinematic variable. Occasionally, the minimum value of q^2 will be negative, which is unphysical. In this case, we set $q^2_{\rm min} = 0$ before computing the average.

The resulting resolution in each variable is good and is significantly improved over the calculation in which the B motion is ignored. The resolutions are q^2 dependent, with typical values $\sigma(q^2) \approx 0.5\ \mathrm{GeV}^2/c^4$, $\sigma(\cos\theta_\ell) \approx 0.07$, $\sigma(\cos\theta_V) \approx 0.07$, $\sigma(\chi) \approx 0.24$. None of these is negligible, however, and we therefore use a fitting method that takes the smearing into account.

In addition to smearing, the fit must also take into account detector acceptance. The most important acceptance effects are the poor detection efficiency for charged pions with momenta below about 100 MeV$/c$ and the low-momentum cutoff for leptons. The soft-pion acceptance effect is particularly important at high q^2, where the D^* is moving slowly. The shape of the soft-pion acceptance has been measured in the data using $D^* \to D^0\pi^+$ decays produced in continuum events.

A similar acceptance effect arises for leptons: leptons produced in the forward direction in the W rest frame are Lorentz boosted to a higher momentum than those produced in the backward direction, for a fixed value of q^2. The cutoff in efficiency for low-momentum leptons directly affects the distribution of $\cos\theta_\ell$, since the efficiency for backward-going leptons ($\cos\theta_\ell < 0$) is very low.

V. FITTING METHOD AND CONSTRAINTS

The joint distribution in q^2, $\cos\theta_\ell$, $\cos\theta_V$, and χ is fit using the unbinned maximum likelihood method. To fully incorporate detector smearing and acceptance effects, we use a Monte Carlo technique [37] to evaluate the likelihood function. The likelihood of the data sample is calculated, for any given set of theoretical parameters, by computing the density of Monte Carlo events around each data point, where the Monte Carlo events are distributed according to the theoretical parameters under consideration. To avoid the need to generate separate Monte Carlo samples for every set of theoretical parameters considered by the fitter, we reweight a single Monte Carlo sample so that the weighted events give the correct density about each data point. This procedure allows us to incorporate the acceptance and smearing effects automatically, since these are modeled by the Monte Carlo.

Although our data sample is much larger than those used in previous analyses, we must still constrain the fit to obtain statistically meaningful results. We are able to extract three parameters, which we select based on the considerations described below. We note that previous analyses, including form factor measurements of D semileptonic decays, have extracted results on at most two parameters apart from the overall rate.

Since the range of D^* recoil velocities is rather small ($w - 1 \leq 0.5$), the form factors are expected to have approximately linear behavior. Within the framework of this assumption, the ideal fit would have five parameters: the ratios $R_1(1)$ and $R_2(1)$ and three form-factor slopes. In studies of $D \to K^*\ell^+\nu$ these slopes are effectively fixed by the assumed pole masses. In our analysis, however, we fit for the slope of h_{A_1}, assuming the linear form

$$h_{A_1}(w) = 1 - \rho^2_{A_1}(w-1). \tag{9}$$

We assume that R_1 and R_2 are constant, so that the free parameters in the fit are $R_1(1)$, $R_2(1)$, and $\rho^2_{A_1}$. Alternative forms for h_{A_1} that have positive curvature would result in higher values of the slope at $w = 1$. Because the range of w is small, our fit is sensitive primarily to the average slope over the full w range and has little sensitivity to curvature.

In reality, R_1 and R_2 are expected to have a mild dependence on w. However, two calculations [8,12] indicate that this departure from heavy-quark symmetry is small. Since the symmetry-breaking corrections to the values of R_1 and R_2 at $w = 1$ are expected to be larger, it is more useful, with present-size data samples, to fit for these quantities. We will test the sensitivity of our values of $R_1(1)$, $R_2(1)$, and $\rho^2_{A_1}$ to this assumption by performing alternative fits in which the predicted w dependence of R_1 and R_2 is used.

The largest background in the analysis, events with fake D^*'s, is explicitly included in the fit. The normalization is determined from the $D^* - D$ sideband as discussed earlier. The shapes of the distributions for the kinematic variables (including their correlations) are obtained with $\Upsilon(4S) \to B\bar{B}$ Monte Carlo, since large samples are required to evaluate the likelihood function. However, we have compared the kinematic distributions predicted from this Monte Carlo with those measured from the data $D^* - D$ sideband and have found excellent agreement. We have also determined that the systematic error associated with the uncertainty on the shapes of the distributions of this background is very small.

The background from the uncorrelated D^*–lepton events is also incorporated into the fit as an additional term in the fitting function. Its normalization is measured from the data. The $B \to D^{**}\ell\nu$ background is treated differently. A term is not included directly in the fitting function, but we use Monte Carlo events to evaluate a small systematic shift that is caused by omitting this background in the fit. We have used ISGW form-factor predictions [13] to model in detail the kinematic distributions for $B \to D_1\ell^-\overline{\nu}$, $B \to D_2^*\ell^-\overline{\nu}$, and $B \to 1^{1/2}P_1\ell^-\overline{\nu}$. Many of the distributions are far from uniform, especially those for the D_1. These modes are expected to occur largely at low q^2, leading to a large helicity-zero component of the D_1 or D_2^*. In addition, the D_1 is expected (and measured by CLEO) to decay in nearly a pure D-wave, resulting in a $1 + 3\cos^2\theta$ distribution of the D in the D^* frame, independent of the D_1 polarization.

VI. FIT RESULTS

Figures 3(a) and 3(b) show the data distributions for q^2 and $\cos\theta_\ell$ after all cuts are applied. The data shown are the combined $D^0 \to K^-\pi^+$ and $D^0 \to K^-\pi^+\pi^0$ modes and include both electrons and muons. The dotted line in each histogram shows the relevant projection of the fit; all projections agree well with the data. The contribution from fake D^{*+} and uncorrelated D^{*+}-lepton events is shown as a dashed line. To help interpret these plots visually, we show in Figures 3(c) and 3(d) the shapes of the q^2 and $\cos\theta_\ell$ distributions calculated using the values of parameters obtained from the fit, but for a detector with perfect acceptance. Also shown are the shapes of the acceptance curves in the electron and muon channels.

Figures 4(a) and 4(b) show the observed distributions for $\cos\theta_V$ in the lower and upper half of the q^2 range. At low q^2, the lepton and neutrino are nearly parallel, forcing the D^* to have helicity zero; this in turn introduces a strong $\cos^2\theta_V$ component in this region of phase space. (The lack of symmetry in this variable is due to poor acceptance for very slow pions.) As q^2 increases, the other helicity components contribute as well, and at q^2_{max} the D^* must be unpolarized.

Figures 4(c) and 4(d) show an interesting correlation between $\cos\theta_V$ and χ. This correlation is produced by the interference term proportional to $(H_+(q^2) - H_-(q^2))H_0(q^2)$. The difference between H_+ and H_- results from the higher probability for the daughter c-quark to have helicity $-1/2$ than helicity $+1/2$. If the coupling at the W vertices were $(V \mp A) \times (V \pm A)$ the slopes in Figures 4(c) and 4(d) would be reversed; for $(V \pm A)(V \pm A)$ they would be the same as what we observe.

All observed distributions are described well by the fit. The values of R_1, R_2, and $\rho^2_{A_1}$ that we obtain are given in Table II. Because there are large correlations among their errors, we also give the off-diagonal terms of the correlation matrix. The corrections are due primarily to the finite volume sizes used in the four-dimensional Monte Carlo likelihood calculation; we obtain these corrections by fitting Monte Carlo samples and comparing measured with generated parameter values. We emphasize that the data are not binned in the likelihood

	R_1	R_2	$\rho^2_{A_1}$
Uncorrected fit	1.25 ± 0.30	0.67 ± 0.22	0.92 ± 0.15
Correction	-0.07	0.04	-0.01
Corrected fit	$1.18 \pm 0.30 \pm 0.12$	$0.71 \pm 0.22 \pm 0.07$	$0.91 \pm 0.15 \pm 0.06$

TABLE II. The first row in the table shows the uncorrected result of the fit. The second line is the correction that is derived from the effect of the finite volume sizes in the fit and the contamination of the $B \to D^{**}\ell\nu$. The errors on the estimated parameters are strongly correlated. The fit estimates the following correlations: $\rho_{R_1R_2} = -0.82$, $\rho_{R_1\rho^2} = 0.60$, and $\rho_{R_2\rho^2} = -0.80$.

fit; rather, the Monte Carlo calculation of the likelihood involves the use of discrete volume sizes around each data point. The remaining part of the correction is due to the effect of $B \to D^{**}\ell\nu$ background.

To test the sensitivity of the fit to the assumption that R_1 and R_2 are constants, we perform alternative fits in which we allow them to vary according to theoretical predictions of Neubert [8] and Close and Wambach [12]. Relative to our standard fit, using the Neubert prediction produces an increase in $R_1(1)$ of 0.06 and a decrease in $R_2(1)$ of 0.06, while $\rho^2_{A_1}$ is essentially unchanged. With the predictions of Close and Wambach, we find an increase in $R_1(1)$ of 0.02 and a decrease of 0.01 in $R_2(1)$, with $\rho^2_{A_1}$ again unchanged.

The systematic errors on the fit results are given in Table III. The uncertainty in shape of the slow-pion detection efficiency as a function of momentum affects the q^2 distribution and hence primarily $\rho^2_{A_1}$. The errors on the three fit parameters are determined by reweighting the Monte Carlo events according to modified slow-pion efficiency functions. The efficiency function, which is measured using data as discussed earlier, is modified according to the 1σ uncertainty on the parameters describing the shape of the curve. A similar reweighting procedure is performed to estimate the sensivity to the uncertainty in lepton identification efficiency.

The uncertainty due to Monte Carlo statistics arises from the finite size of the sample used to calculate the likelihood function, and is determined by performing fits using several independent Monte Carlo samples. The correction due to finite volumes used in the likelihood function calculation was described above; the uncertainty in this correction arises from the finite Monte Carlo sample used to evaluate the correction.

Our fits include the uncorrelated D^{*+}–lepton background in the fitting function. The systematic error here is due to the uncertainty in the number of such events, as determined from data in the sample of events with the D^* and lepton in the same hemisphere. Finally, the δm sideband error is due to several sources: the uncertainty in the number of fake D^* events, as measured from the sideband; the error due to finite Monte Carlo sample used in evaluating the likelihood; and the uncertainty in the Monte Carlo modeling of the shapes of the distributions.

The δm efficiency error is the uncertainty associated with the efficiency of our $\delta m = M(D^{*+}) - M(D^0)$ cut as a function of q^2. Because this cut is rather tight ($\approx 2\sigma$), incorrect modeling of the efficiency could introduce an error in measuring the q^2 distribution.

	R_1	R_2	$\rho^2_{A_1}$
Slow pion efficiency	0.01	0.01	0.04
Finite MC statistics	0.03	0.01	0.01
Finite volumes	0.05	0.04	0.03
$B \to D^{**}\ell\nu$	0.08	0.04	0.02
Lepton efficiency	0.02	0.02	0.01
Uncorr. Background	0.03	0.01	0.01
δm-sideband	0.05	0.03	0.02
δm efficiency	0.01	0.01	0.02
Total	0.12	0.07	0.06

TABLE III. Systematic errors on R_1, R_2, and $\rho^2_{A_1}$.

To compare with previous measurements of the lepton forward-backward asymmetry, $\bar{A}_{\rm FB}$, and the D^* polarization, $\bar{A}_{\rm pol}$, we calculate these quantities from the result of the three parameter fit. We obtain $\bar{A}_{\rm FB} = 0.197 \pm 0.033 \pm 0.016$ and $\bar{A}_{\rm pol} = 1.55 \pm 0.26 \pm 0.13$, compared with the ARGUS results [28] of $\bar{A}_{\rm FB} = 0.20 \pm 0.08 \pm 0.06$ and $\bar{A}_{\rm pol} = 1.1 \pm 0.4 \pm 0.2$. For the value $\rho^2 = 1.0$, Neubert calculates [8] $\bar{A}_{\rm FB} = 0.22$ and $\bar{A}_{\rm pol} = 1.37$.

VII. CONCLUSIONS

We have measured the form factors for the process $\bar{B}^0 \to D^{*+}\ell^-\overline{\nu}$ using an unbinned maximum likelihood fit. Three parameters are determined from the fit, two form-factor ratios R_1 and R_2, and the form-factor slope $\rho^2_{A_1}$. The ratios R_1 and R_2 differ somewhat from the traditional definitions used in D semileptonic decays in that their relative q^2 dependence is consistent with constraints from heavy-quark symmetry. The q^2 dependence of each of the three form factors is assumed to be related by heavy-quark symmetry to the form factor h_{A_1}, which becomes the Isgur-Wise function in the heavy-quark symmetry limit, and which we take to be a linear function of q^2: $h_{A_1}(w) = 1 - \rho^2_{A_1}(w-1)$, where w measures the D^* recoil velocity and is defined after Eq. 3.

With these assumptions, we obtain the preliminary form factor ratios $R_1(1) = 1.18 \pm 0.30 \pm 0.12$ and $R_2(1) = 0.71 \pm 0.22 \pm 0.07$, which can be compared with the heavy quark symmetry limit of $R_1(1) = R_2(1) = 1$. Our values agree well with the predictions of Neubert [8], $R_1(1) = 1.35$ and $R_2(1) = 0.79$, and Close and Wambach [12], $R_1(1) = 1.15$ and $R_2(1) = 0.91$. The errors on our measurements are highly correlated, as discussed in the previous section. In the same fit, we determine the slope of $h_{A_1}(w)$ to be $\rho^2_{A_1} = 0.91 \pm 0.15 \pm 0.06$. Since we assume a linear form, this parameter measures the average slope over the w range. This value is consistent with the range 0.5 to 2.0 expected from calculations using lattice QCD and QCD sum rules.

The comparison of this measurement of $\rho^2_{A_1}$ with that from the CLEO II V_{cb} measurement [32] using $B \to D^*\ell\nu$ requires some care. That measurement uses a standard procedure in which the $d\Gamma/dq^2$ distribution is fit to a function that assumes $R_1 = R_2 = 1$. For this reason, Neubert refers to the slope parameter obtained from the $d\Gamma/dq^2$ fit as $\hat{\rho}^2$. Using the relation [9]

$$\Delta\rho^2 = \hat{\rho}^2 - \rho^2_{A_1} = -\frac{1}{6}(R_1^2 - 1) - \frac{1}{3}\frac{m_B}{m_B - m_{D^*}}(1 - R_2), \qquad (10)$$

we find $\rho^2_{A_1} \approx \hat{\rho}^2 + 0.22$. The CLEO II value of $\hat{\rho}^2$ is $0.84 \pm 0.13 \pm 0.08$, which would correspond to a value of $\rho^2_{A_1}$ around 1.06. Thus, the CLEO II $\rho^2_{A_1}$ and $\hat{\rho}^2$ measurements appear to be consistent.

Our method for determining the $B \to D^*\ell\nu$ form factors is significantly different from previous studies. Earlier measurements have fit for at most two of the three parameters in our fit. Because of our large data sample and because we use the powerful information in the correlations among all the kinematic variables, we are able to fit simultaneously for all three parameters. In the previous CLEO II measurement [30], the lepton forward-backward asymmetry $\bar{A}_{\rm FB}$ was measured, and the form factors were extracted by performing a χ^2 fit to $\bar{A}_{\rm FB}$ and to both ARGUS and CLEO measurements of $\bar{A}_{\rm pol}$ and $d\Gamma/dq^2$. In that study, the q^2 dependence of the form factors was fixed. In the ARGUS measurement [28], the quantities $\bar{A}_{\rm FB}$ and $\bar{A}_{\rm pol}$ are quoted but not the form factors. In studies [28,32,31] of the $d\Gamma/dq^2$ distribution that are used to determine $|V_{cb}|$, a slope is determined that is closely related to $\rho^2_{A_1}$. However, these measurements assume the heavy-quark symmetry limit, $R_1 = R_2 = 1$.

One of the important results of our new fit is that the corrections to the heavy-quark symmetry limit do indeed appear to be fairly small. This result provides confidence in the use of heavy-quark symmetry as a starting point for the extraction of $|V_{cb}|$ from $B \to D^*\ell\nu$. Although our study is more general than previous ones, we have still made the important assumption that the q^2 dependence of each of the three form factors can be related to a single function. Substantially more data will be required before one can allow each of the three form factors to have a separate dependence on q^2 in the fit.

We also observe a large effect produced by the interference terms in the decay amplitude, indicating a large difference in the amplitude for producing the W in helicity $+1$ and -1 states. This correlation helps to improve our measurement of R_1 and has not previously been used. The correlation is consistent with $(V - A)$ couplings at both W vertices.

ACKNOWLEDGEMENTS

We gratefully acknowledge the effort of the CESR staff in providing us with excellent luminosity and running conditions. This work was supported by the National Science Foundation, the U.S. Department of Energy, the Heisenberg Foundation, the Alexander von Humboldt Stiftung, the Natural Sciences and Engineering Research Council of Canada, and the A.P. Sloan Foundation.

REFERENCES

[1] J. Richman and P. Burchat, to be published in Rev. Mod. Phys. (1995).

[2] N. Isgur and M.B. Wise, Phys. Lett. B **232**, 113 (1989).

[3] N. Isgur, and M.B. Wise, Phys. Lett. B **237**, 527 (1990).

[4] M.E. Luke, Phys. Lett. B **252**, 447 (1990).

[5] C.G. Boyd and D.E. Brahm, Phys. Lett. B **257**, 393 (1991).

[6] M. Neubert, Phys. Lett. B **264**, 455 (1991).

[7] M. Neubert and V. Rieckert, Nucl. Phys. B **382**, 97 (1992).

[8] M. Neubert, Phys. Reports **245**, 259 (1994).

[9] M. Neubert, Phys. Lett. B **338**, 84 (1994)

[10] T. Mannel, Phys. Rev. D **50**, 428 (1994).

[11] M. Shifman, N.G. Uraltsev, and A. Vainshtein, Phys. Rev. D **51**, 2217 (1995).

[12] F.E. Close and A. Wambach, Rutherford Lab. Preprint No. RAL-94-041 (1994).

[13] N. Isgur, D. Scora, B. Grinstein, and M.B. Wise, Phys. Rev. D **39**, 799 (1989).

[14] D. Scora and N. Isgur, CEBAF Preprint No. CEBAF-TH-94-14 (1994).

[15] J.G. Körner and G.A. Schuler, Z. Phys. C **38**, 511 (1988) [Erratum: C **41**, 690 (1989)].

[16] J.G. Körner and G.A. Schuler, Z. Phys. C **46**, 93 (1990).

[17] M. Wirbel, B. Stech, and M. Bauer, Z. Phys. C **29**, 637 (1985).

[18] M. Bauer and M. Wirbel, Z. Phys. C **42**, 671 (1989).

[19] C. Bernard, Y. Shen, and A. Soni, Phys. Lett. B **317**, 164 (1993).

[20] S.P. Booth, *et al.* (UKQCD), Phys. Rev. Lett. **72**, 462 (1994).

[21] J.D. Bjorken, in *Results and Perspectives in Physics, Proceedings of the 4th Rencontres de Physique de la Valle d'Aoste, La Thuile, Italy* ed. by M. Greco (Editions Frontières, France), p. 583 (1990); and *Proceedings of the Eighteenth SLAC Summer Institute on Particle Physics, Gauge Bosons and Heavy Quarks, July 1990*, edited by J.F. Hawthorne, SLAC-Report-378, p. 167 (1991).

[22] B. Blok and M. Shifman, Phys. Rev. D **47**, 2949 (1993).

[23] M.B. Voloshin, Phys. Rev. D **46**, 3062 (1992).

[24] H.Y. Jin, C.S. Huang, and Y.B. Dai, Z. Phys. C **56**, 707 (1992).

[25] S. Narison, Phys. Lett. B **325**, 197 (1994).

[26] Y. Kubota *et al.* (CLEO), Nucl. Instrum. Methods A **320**, 66 (1992).

[27] R.J. Morrison and J.D. Richman, "Note on Semileptonic Decays of D and B Mesons," Part I, p. 1565 and Part II, p. 1602, in *Review of Particle Properties,* Phys. Rev. D **50**, 1173 (1994).

[28] H. Albrecht *et al.* (ARGUS), Z. Phys. C **57**, 533 (1993).

[29] D. Bortoletto, *et al.* (CLEO), Phys. Rev. Lett. **63**, 1667 (1989).

[30] S. Sanghera *et al.* (CLEO), Phys. Rev. D **47**, 791 (1993).

[31] ALEPH Collab., ICHEP Ref. 0605, paper submitted to the 27th International Conference on High Energy Physics, Glasgow, Scotland, July 20–27, 1994.

[32] B. Barish *et al.* (CLEO), Phys. Rev. D **51**, 1014 (1995).

[33] D. Buskulic *et al.* (ALEPH), Phys. Lett. B **345**, 103 (1995).

[34] Hadronic events must have at least 3 charged tracks originating near the interaction point, and the total visible energy in the calorimeter for the event must be greater than $0.15E_{\rm CM}$, where $E_{\rm CM}$ is the center-of-mass energy.

[35] G. Fox and S. Wolfram, Phys. Rev. Lett. **41,** 1581 (1978).

[36] J.C. Anjos *et al.* (E691), Phys. Rev. D **48**, 56 (1993).
[37] D.M. Schmidt, R.M. Morrison, and M. Witherell, Nucl. Instrum. Methods A **328**, 547 (1993).

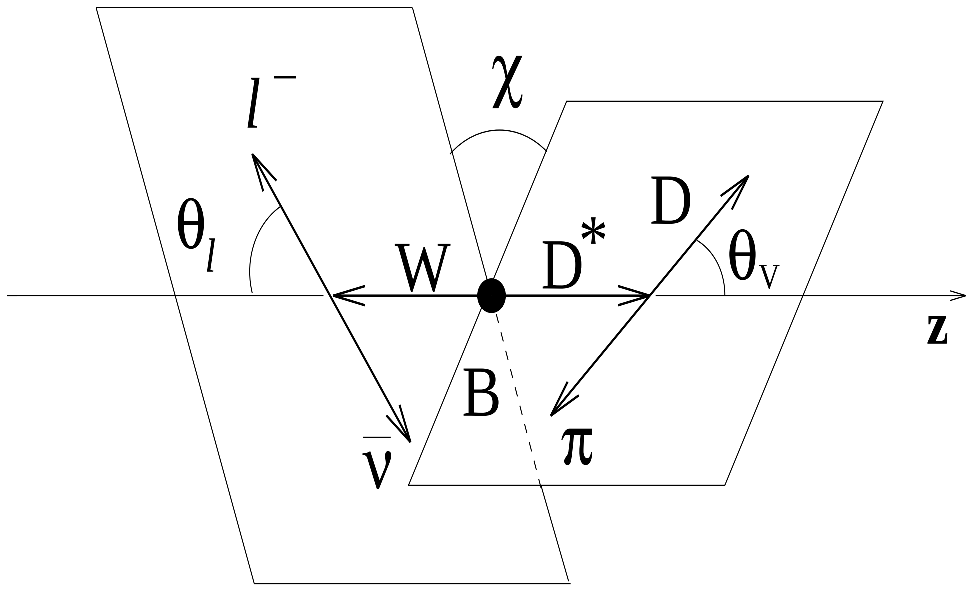

FIG. 1. Definition of the angles $\cos\theta_\ell$, $\cos\theta_V$, χ. The polar angles θ_ℓ and θ_V are defined in the rest frames of the virtual W and the D^*, respectively, and χ is the azimuthal angle between the projections of the lepton and D momentum vectors in the plane perpendicular to z.

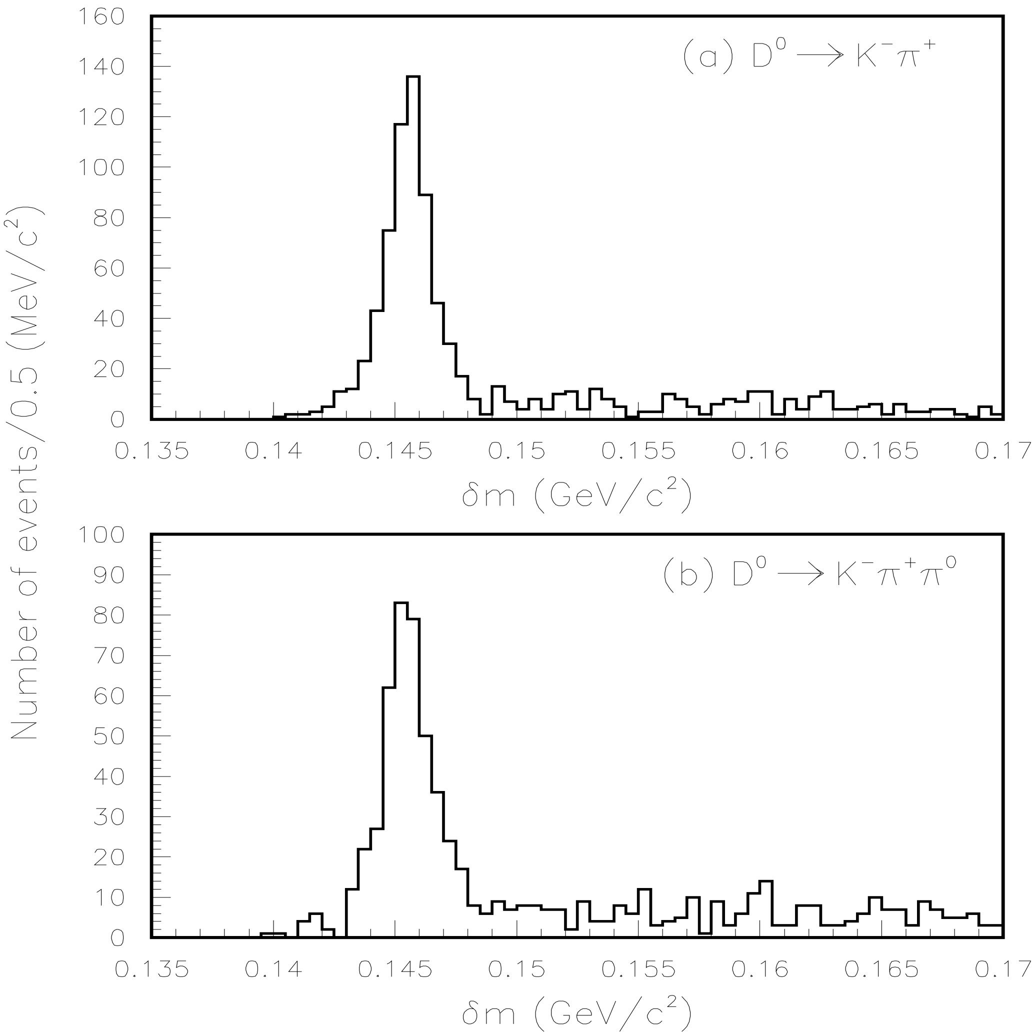

FIG. 2. The distribution of $\delta m = M(D^{*+}) - M(D^0)$ for (a) $D^0 \to K^-\pi^+$ candidates and (b) $D^0 \to K^-\pi^+\pi^0$ after all analysis cuts except the δm cut.

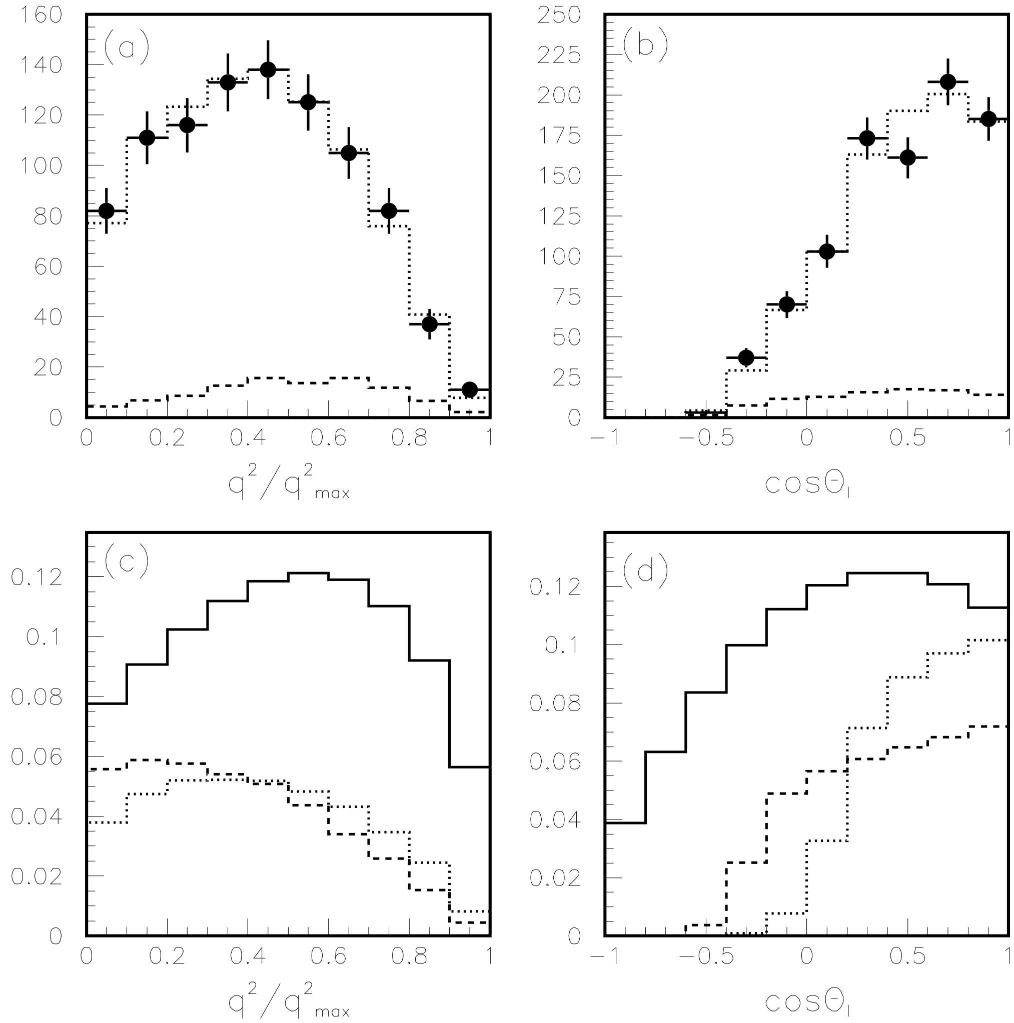

FIG. 3. The distributions of (a) q^2 and (b) $\cos\theta_\ell$ after all cuts. The points with error bars are the data, and the dotted histogram shows the result of the fit. The dashed line shows the contribution of the two backgrounds included in the fit: fake D^{*+}'s and uncorrelated D^{*+}–lepton pairs. These histograms include both $D^0 \to K^-\pi^+$ and $D^0 \to K^-\pi^+\pi^0$ channels, electrons and muons. In (c) and (d), we show the distributions that would be observed by a perfect detector (solid) and the shapes of the acceptance for electrons (dashed curves) and muons (dotted curves).

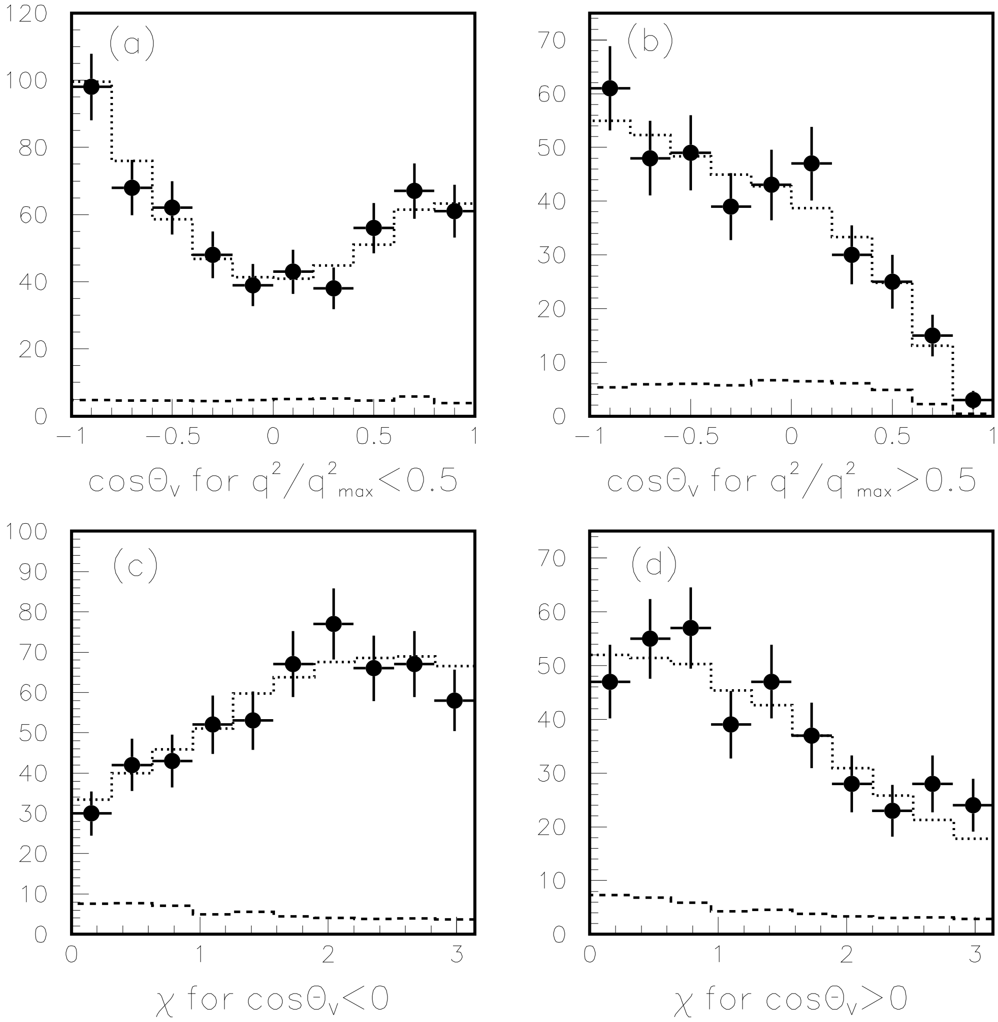

FIG. 4. Distributions of $\cos\theta_V$ for the (a) lower half and (b) upper half of the q^2 range. At low q^2, the longitudinal component of the D^* dominates. At $q^2_{\rm max}$, the D^* is unpolarized. The dotted lines in the histograms show the result of the fit, and the dashed lines show the background from fake D^{*+}'s and uncorrelated D^{*+}-lepton events. Figures (c) and (d) show the χ distributions for $\cos\theta_V < 0$ and $\cos\theta_V > 0$, respectively.